Non-spontaneous and multilayer adsorption of malachite green dye by *Acacia nilotica* waste with dominance of physisorption

M. T. Amin, A. A. Alazba and M. Shafiq

ABSTRACT

Adsorption of the hazardous dye malachite green (MG) by *Acacia nilotica* (AN) waste was investigated. Batch process variables for the adsorption of MG by AN were optimized. The mechanisms involved in the adsorption of MG by AN were explored using isotherms and kinetic models. The thermodynamic parameters were calculated to determine the spontaneity and thermal nature of the MG adsorption reaction. The maximum equilibrium adsorption capacity of AN was found to be 113.26 mg/g at 30 °C. The MG adsorption data revealed that AN adsorbs MG by multilayer adsorption, as shown by the better fit of the data to the Freundlich and Halsey models ($R^2 = 0.99$) rather than to the Langmuir model. Multilayer adsorption involves physisorption, which was confirmed by the *E*-value of the Dubinin-Radushkevich model (6.52 kJ/mol). Surface diffusion was found to be the main driving force for MG adsorption by AN. The MG adsorption reaction was endothermic, based on the enthalpy, and was controlled by the entropy of the system in the T_1 temperature range (30 to 40 °C), while the opposite trend was observed in the T_2 range (40 to 50 °C). Moreover, MG adsorption by AN was found to be nonspontaneous at all temperatures.

Key words | *Acacia nilotica*, malachite green dye, nonspontaneous adsorption, surface diffusion

M. T. Amin (corresponding author)
A. A. Alazba
M. Shafiq
Alamoudi Water Research Chair,
King Saud University,
P.O. Box 2460,
Riyadh 11451,
Kingdom of Saudi Arabia
E-mail: *mtamin@ksu.edu.sa*

M. T. Amin
Department of Environmental Sciences,
COMSATS Institute of Information Technology,
Abbottabad 22060,
Pakistan

A. A. Alazba
Agricultural Engineering Department,
King Saud University,
P.O. Box 2460,
Riyadh 11451,
Kingdom of Saudi Arabia

INTRODUCTION

Malachite green (MG) is a cationic dye, being positively charged in aqueous solution, and belongs to the triarylmethane dye class. This dye has been used to control diseases and parasites in fish farms (Zhang *et al.* 2008) because of its properties as a disinfectant and ectoparasiticide. In addition, MG is used to color silk, cotton, and leather (Gupta *et al.* 2004; Kumar *et al.* 2005). However, this dye can damage aquatic life via its carcinogenic and mutagenic properties, which have been confirmed in animal model studies (Culp *et al.* 1999; Srivastava *et al.* 2004; Yonar & Yonar 2010). Moreover, the intense color of this dye imparts an unpleasant color to water bodies, and it is recalcitrant to degradation by light and other oxidizing agents, increasing environmental concerns and making its removal problematic.

Conventional methods of chemical precipitation (Gao *et al.* 2007), advanced oxidation (Azbar *et al.* 2004; Yetilmezsoy & Sakar 2008), and biological oxidation (Kapdan *et al.* 2000; Ghoreishi & Haghighi 2003) have been used to remove contaminating dyes from water, but, for dilute concentrations of dyes, their use is not practical. Moreover, foam filtration (Lu *et al.* 2010) and flocculation (Wei *et al.* 2009; Riera-Torres *et al.* 2010) have also been used to remove dyes from textile industrial waste, but these methods are also ineffective. Therefore, over the last two decades, focus has shifted towards using adsorption techniques for removing hazardous dyes because of their effectiveness and low cost (Kant 2012; Amin *et al.* 2016). Adsorption techniques are more economical than their alternatives if the adsorbent is indigenous to the treatment area and requires no treatment prior to its application to wastewater treatment (Amin *et al.* 2015). Although many bioadsorbents have been used for the removal of MG dyes from aqueous streams, for example, sugarcane waste (Kattri & Singh 1999), neem sawdust (Khattri & Singh 2000), maize cob (Sugumar & Gopalan 2000), Parthenium weed (Rajeshwarisivaraj & Subburam 2002), jackfruit peel (Inbaraj & Sulochana 2002), fresh water algae (Kumar *et al.* 2005), rice husks (Guo *et al.* 2003), fly ash (Janoš *et al.* 2003), and spent tea leaves (Akar *et al.* 2013), the search for low-cost waste

doi: 10.2166/wst.2017.366

materials to remove hazardous dyes from waste streams prior to disposal continues. Furthermore, the use of these waste materials is important from an economic point of view (Hameed *et al.* 2008).

This study focused on the use of *Acacia nilotica* (AN) sawdust for the removal of MG in batch experiments. AN is a waste adsorbent which is generated from the wood industry, and AN wood sawdust is abundantly available in wood processing industry as a solid waste material (Jain *et al.* 2011). In this study, we optimized various process variables, and kinetics and isotherm studies were performed to elucidate the mechanism of MG dye adsorption. In addition, thermodynamic parameters were calculated to determine the stability of the material and the spontaneity and thermal nature of the MG dye adsorption reactions.

MATERIALS AND METHODS

The chloride salt of MG was used as the model pollutant in this study. A stock solution of 1,000 mg/L was prepared, and, subsequently, the working solutions were prepared by the dilution of the stock solution with deionized water.

Collection and preparation of the waste adsorbent

AN waste biomass was collected from local wood companies in the Kingdom of Saudi Arabia. The adsorbent was washed with deionized water, dried, ground, and sieved, and the required mesh sizes were used in the batch experiments.

Characterization of the AN adsorbent

Scanning electron microscopy (SEM, HITACHI S-3000N, JAPAN) analysis was conducted to analyze the texture of the AN adsorbent material before MG dye loading. Furthermore, the porosity of the AN surface was analyzed from the SEM micrographs taken before MG dye loading and at various magnifications (250×, 500×, and 1,000×). These micrographs were taken at a 5-kV acceleration voltage, and a 25-mm working distance was maintained. Moreover, energy dispersive X-ray (EDX) analysis was performed to determine the elemental composition of the AN adsorbent. Fourier-transform infrared (FTIR) measurements were made (model 460 plus) in the region of 4,000–400 cm^{-1}, and the types of functional groups on the surface of the AN adsorbent were determined before MG dye loading.

Batch adsorption studies

Batch adsorption studies were performed by adding a fixed amount of AN adsorbent (0.05 g) into 100-mL Erlenmeyer flasks. The concentration of MG dye (50 mg/L) was maintained in the 50-mL solution, except for the contact time experiments, where the initial MG dye concentration was 40 mg/L. The MG dye solution pH (7) and particle size of AN adsorbent (400 μm) were also kept constant. The flasks were agitated in a temperature controlled shaking incubator at 220 rpm and 30 °C until equilibrium was reached. Aqueous samples were taken from the shaker, and the concentrations were analyzed at 616 nm by a double beam UV/VIS spectrophotometer (T80$^+$ PG Instruments, UK). The adsorption capacity of AN, q_e (mg/g), and the removal efficiency (%) were calculated using Equations (1) and (2), respectively.

$$q_e = \left(\frac{C_o - C_f}{m}\right) V \tag{1}$$

$$removal\ (\%) = \left(\frac{C_o - C_f}{C_o}\right) \times 100 \tag{2}$$

where C_o and C_f (mg/L) are the liquid-phase dye concentrations at the initial and equilibrium time, respectively. V is the volume of the solution (L), and m is the mass of AN sorbent used (g).

Adsorption isotherms, kinetics, and thermodynamic studies

The experimental data for the adsorption of MG onto AN at initial dye concentrations ranging from 25 to 200 mg/L (Table 1) were fitted with different adsorption kinetic and isotherm models. In contrast, the batch parameters, *i.e.*, pH (7), temperature (30 °C), adsorbent dose (0.05 g/L), shaking speed (220 rpm), and contact time (40 min), were kept constant. We used the Langmuir, Freundlich, Halsey, Dubinin-Radushkevich (D-R), and Temkin isotherm

Table 1 | Thermal parameters for the adsorption of MG dye onto AN

		ΔG (J/mol)				
ΔH/(kJ/mol)	ΔS/(kJ/mol)	303 K	308 K	313 K	318 K	323 K
21.79	0.06	1.24	0.90	0.56	–	–
−30.95	−0.10	–	–	0.50	1.00	1.51

models. Different kinetic theories (the pseudo-second-order kinetic and intraparticle diffusion models) were also applied to explain the driving force behind the mass transfer of the pollutants from the liquid to the solid phases. The corresponding correlation coefficients and constants of the model plots were calculated. Moreover, the Gibbs free energy, enthalpy, and entropy of the MG dye adsorption process were investigated at the solid-solution interface. To analyze the energy of the system and the optimum temperature for MG adsorption, the Gibbs free energy (ΔG, kJ/mol), enthalpy (ΔH, kJ/mol), and entropy (ΔS, kJ/mol) of the reaction system were studied. For this purpose, equilibrium adsorption studies of MG dye onto AN were carried out at variable temperatures (30, 35, 40, 45, and 50 °C), while keeping the dye concentration fixed at 50 mg/L, the adsorbent dose at 0.5 g/L, the pH at 7, and the agitation at 220 rpm. The enthalpy and entropy of the system was calculated from the slope × R and intercept × R of the ($\ln K_d$ vs. $1/T$) plot, where R is the universal gas constant. The Gibbs free energy was calculated using Equation (5).

Statistical analysis

Multiple replicates (minimum 3) for each batch experiment were conducted, and the data are presented as the mean ± standard error. The one-way analysis of variance was performed to analyze the effects of different variables on the MG adsorption capacity of the AN adsorbent. Different letters on the mean error bar indicated the least significant difference of means at $p = 0.01$.

RESULTS AND DISCUSSIONS

SEM and EDX analyses of the AN adsorbent

Textural and elemental analysis of the AN adsorbent was carried out before and after MG adsorption (Figure 1(a) and 1(b)). SEM micrographs of the AN adsorbent were taken at various magnifications. The image at 1,000× shows the rough and uneven surface morphology with prominent primary and secondary pores. These pores could be involved in the uptake of MG.

EDX analysis revealed the elemental composition by weight of the AN adsorbent: C (58.22%), O (41.46%), and Al (0.12%) (see Figure 1(c)). After MG loading onto the AN surface (Figure 1(d)), the increases in C (59.12%), N (4.73%), and O (43.87%) contents confirmed that the dye has been successful adsorbed on the adsorbent surface.

FTIR studies

FTIR studies were carried out for the determination of functional groups on the AN surface. The FTIR spectra of AN before and after the loading of MG are shown in Figure 2.

The peak at 3,616 cm^{-1} is pertinent to O-H stretching vibrations (Wu *et al.* 2016). The band at 2,216 cm^{-1} might be due to –C ≡ N- stretching vibrations. The reduction in peak intensity at 3,616 and 2,216 cm^{-1} indicates the formation of interactions with the hydroxyl and nitrile groups, respectively, during the adsorption of MG onto AN (Shakoor & Nasar 2016).

Optimization of batch process variables

Effects of the contact time on the adsorption of MG by AN

A series of batch experiments was conducted as a function of contact time, and the time to reach equilibrium determined the minimum time required for the adsorption of MG by AN (Figure 3(a)). The MG dye removal mechanism can be described as the transfer of dye molecules from the liquid phase to the AN particles, as well as by surface diffusion. The effect of contact time on the removal of MG was studied in a solution containing 40 mg/L MG dye and 0.05 g/L of adsorbent. The data reveal the increasing removal of MG dye from 12 mg/g (30.05%) to 15.19 mg/g (38%) with increasing contact time, *i.e.*, from 20 to 240 min (Figure 3(a)). The equilibrium adsorption of the MG dye was reached after 40 min. Afterward, there was no significant ($p = 0.01$) increase in the adsorption of the MG dye. The initial sharp rise is ascribed to the availability of active sites, but the surface of the AN adsorbent becomes saturated with MG dye with increasing time. The effect of the other parameters onto MG adsorption was optimal at the equilibrium time of 40 min.

Effects of pH on the adsorption of MG by AN

MG is a cationic dye and is positively charged in the aqueous phase. Thus, MG is an ionic species, and its adsorption onto the AN surface is primarily influenced by the surface charge of the adsorbent, which in turn is influenced by the solution pH. In this study, the effect of pH on MG adsorption was studied, while the agitation speed, solution temperature, initial dye concentration, amount of AN adsorbent, contact time, and particle size were kept constant. *i.e.*, 220 rpm, 30 °C, 50 mg/L, 0.05 g, 40 min, and 40 mesh, respectively. The effects of pH were investigated

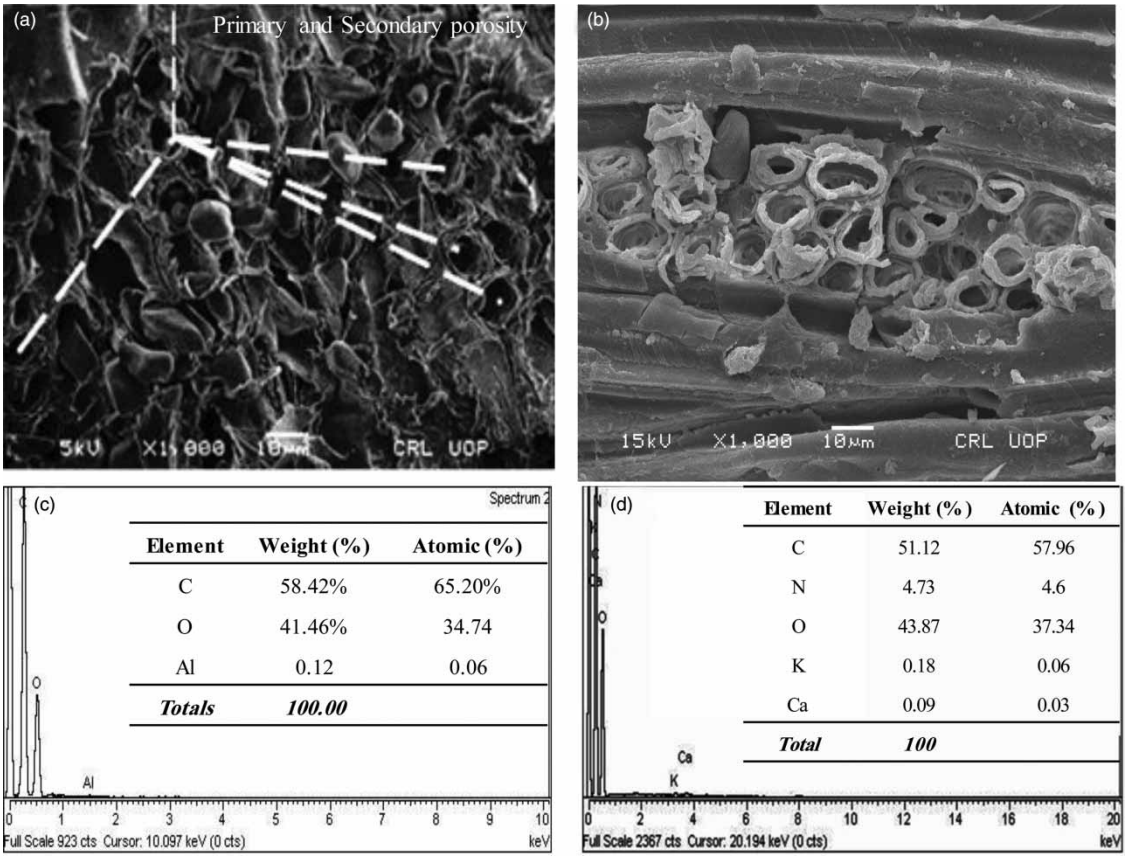

Figure 1 | SEM micrographs (a and b) and EDX analysis (c and d) of the AN adsorbent before MG dye loading.

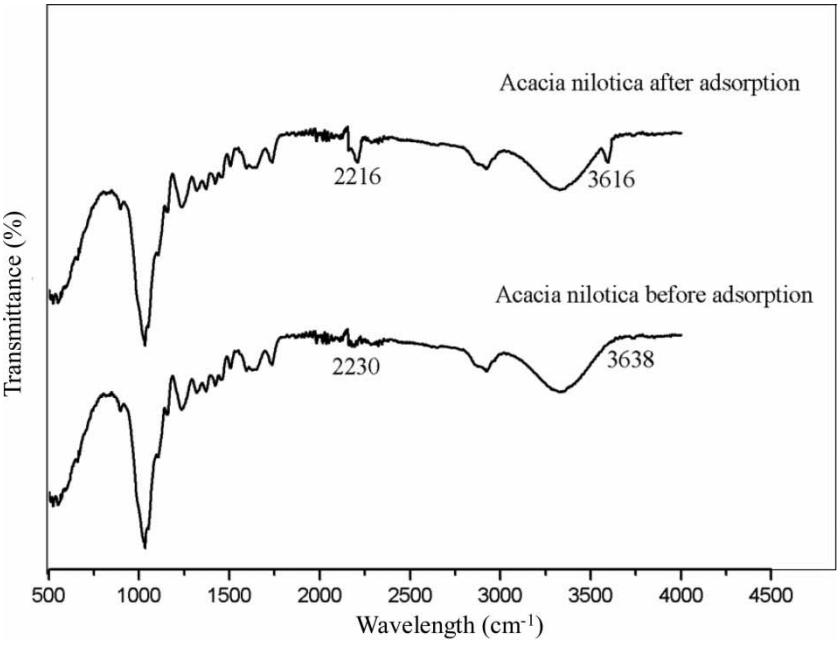

Figure 2 | FTIR spectra before and after MG dye adsorption.

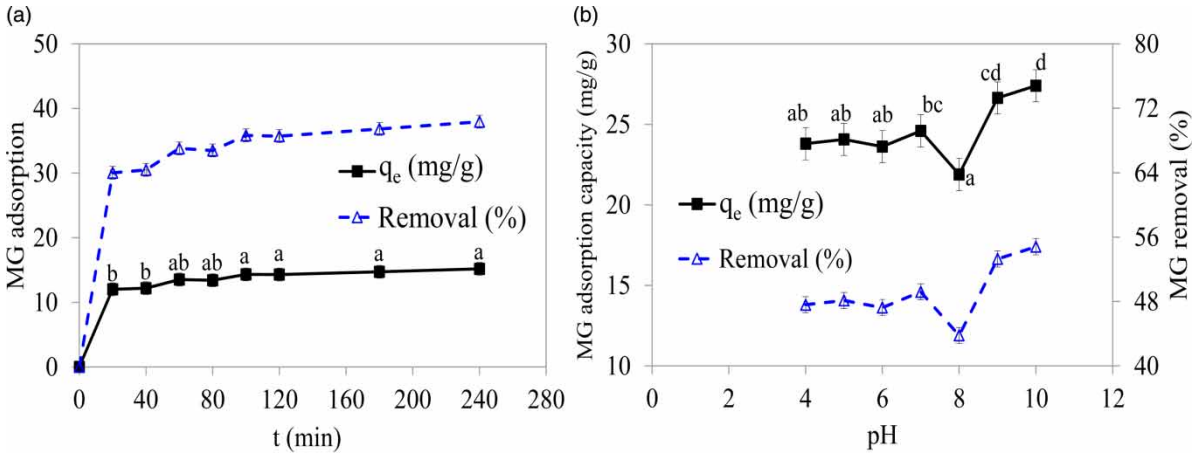

Figure 3 | Effects of contact time (a) and solution pH (b) on the adsorption of MG by AN.

over the pH range of 4 to 10 pH (Figure 3(b)). MG adsorption was found to be significantly ($p = 0.01$) reduced (23.80 mg/g, 47.60%) at low pH (4) compared to that (27.40 mg/g, 54.81%) at high pH (11). This is because the excess H^+ ions at low pH can compete with the positive MG ions for active adsorption sites. In contrast, at high pH, the positive charges at the solid-liquid interface decrease and the adsorbent surface becomes negatively charged; this results in high MG dye removal (Pan & Zhang 2009; Baek *et al.* 2010). Similar pH effects have also been reported for the adsorption of cationic dyes by rattan sawdust (Hameed & El-Khaiary 2008).

Effect of agitation speed on the adsorption of MG by AN

Agitation speed plays a key role in the mass transfer processes during batch adsorption. It had a significant ($p = 0.01$) impact on the adsorption capacity of the AN adsorbent (Figure 4(a)). MG adsorption was increased significantly from 2.28 mg/g (5.70%) at 100 rpm to 12.60 mg/g (31.50%) at 220 rpm. This can be ascribed to the increased turbulence and degree of mixing that reduce the thickness of the boundary layer surrounding the adsorbent particles. Similar observations have been reported in the literature (Fil *et al.* 2014). Therefore, an agitation speed of 220 rpm was selected for the batch adsorption experiments.

Effect of the initial MG dye concentration on its adsorption by AN

The amount of adsorbed MG dye (mg/g) increased with the increasing solution dye concentration. Figure 4(b) shows the high and significant ($p = 0.01$) MG adsorption capacity, 113.26 mg/g (56.63%), of AN at a maximum initial MG dye concentration of 200 mg/L compared to that at a lower initial MG dye concentration of 25 mg/L. The data

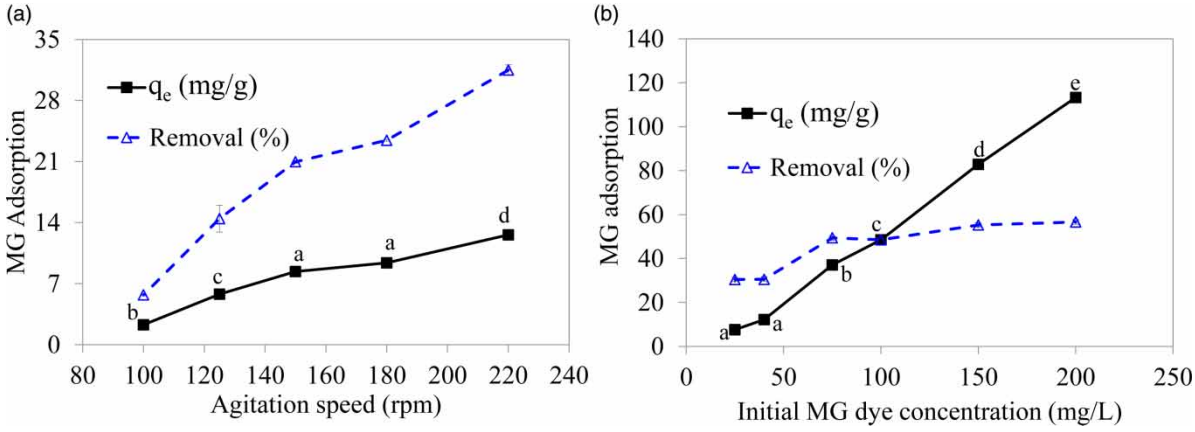

Figure 4 | Effects of the agitation speed (a) and initial MG dye concentration (b) on the adsorption of MG by AN.

show the dependence of the AN adsorption capacity on the initial adsorbate concentration in the solution. The data also reveal that the increasing solute concentration provides a sufficient driving force to control the resistance to mass transfer between the liquid and solid phases.

Temperature and thermodynamics

Effect of temperature on the adsorption of MG by AN was studied over two temperature ranges, T_1 (30 to 40 °C) and T_2 (40 to 50 °C) (Figure 5). In the first temperature range, the temperature effect was significant because the MG adsorption capacity of the AN adsorbent was significantly higher (18.64 mg/g, 37.28%) at 40 °C than that (22.35 mg/g, 44.70%) at 30 °C. However, in the T_2 temperature range, the AN adsorbent displayed a nonsignificant ($p = 0.01$) decreasing trend in the MG adsorption capacity with increasing temperature, *i.e.*, 22.35 mg/g (44.70%) at 40 °C to 20.35 mg/g (40.70%) at 50 °C, respectively.

Among the thermodynamic parameters, the equilibrium constant K_d was calculated from Equation (3).

$$K_d = \frac{q_e}{C_e} \tag{3}$$

where q_e (mg/g) is the equilibrium adsorption capacity and C_e (mg/g) is the liquid phase concentration at equilibrium. This value further used in the Van't Hoff plot. The change in the enthalpy and entropy were calculated from the Van't Hoff plot using Equation (4).

$$\ln K_d = \frac{\Delta S}{R} - \frac{\Delta H}{RT} \tag{4}$$

where ΔH (kJ/mol) is the change in the standard enthalpy, ΔS is the change in the standard entropy (kJ/mol), K_d is the equilibrium constant of adsorption (q_e/C_e), R is the universal gas constant (8.314 J/mol/K), and T is the temperature (K).

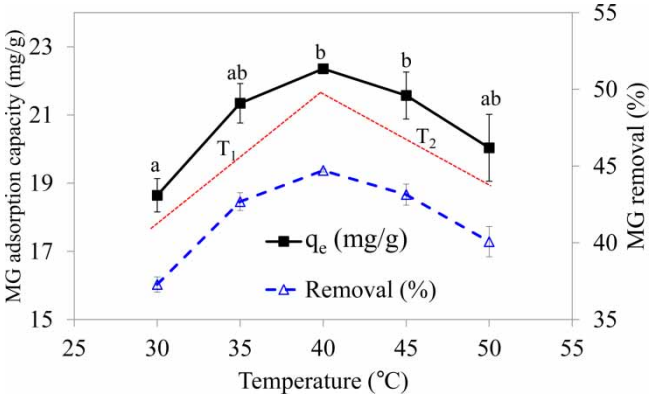

Figure 5 | Effects of the temperature on the adsorption of MG by AN.

In the T_1 temperature range, the value of ΔH was 21.79 kJ/mol, demonstrating the endothermic nature of reaction between the MG dye molecules and the adsorbent surface. The positive value of ΔS (0.06 kJ/mol) confirms the increased disorder at the solid-liquid interface during MG adsorption. This is because the mobility of the adsorbate ions/molecules in the solution increases with increasing temperature. However, the MG adsorption reaction is unfavorable with respect to the enthalpy but favorable with respect to the entropy, indicating that the MG adsorption reaction is an entropy-driven process.

The Gibbs free energy change (ΔG, kJ/mol) values were obtained from Equation (5).

$$\Delta G = \Delta H - T\Delta S \tag{5}$$

The values of ΔG in the T_1 temperature range indicate the nonspontaneous nature of MG adsorption onto the surface of the AN adsorbent. However, the nonspontaneity of the absorption of MG by AN is reflected by the decreasing values of the Gibb's free energies with increasing temperature (Table 1).

In the T_2 temperature range, the values of ΔH and ΔS were found to be −30.95 and −0.01 kJ/mol, respectively (Table 1). These values indicate that the adsorption of MG dye is favorable with respect to the enthalpy of the system but unfavorable with respect to the entropy. The values of ΔG in the T_2 temperature range indicates the nonspontaneous nature of MG adsorption on the surface of the AN adsorbent at all temperatures.

Equilibrium adsorption isotherms

These isotherms are mathematical models for the optimization of an system with extensive applications. These models also indicate the relationship between the contaminant ions that are adsorbed on the adsorbent surface and those present in the solution at equilibrium (Shanmugaprakash *et al.* 2014). The Langmuir (Langmuir 1918), Freundlich (Freundlich 1906), Halsey (Halsey 1948), D-R (Dubinin & Radushkevich 1947), and Temkin (Temkin & Pyzhev 1940) isotherms were employed to elucidate the mechanism of MG adsorption.

The Langmuir model has frequently been applied to study the removal of dyes (Yang & Al-Duri 2005). In the

Langmuir model, a homogeneous distribution of active sites at the surface of the studied adsorbent is assumed; in addition, it is assumed that there are no interactions between adjacent adsorbed dye molecules. The Langmuir model, as expressed in Equation (6a) and can be written in a linearized form, as shown in Equation (6b).

$$q_e = \frac{(q_{\max} K_{ads} C_e)}{1 + K_{ads} C_e} \tag{6a}$$

$$\frac{1}{q_e} = \frac{1}{q_{\max}} + \left(\frac{1}{q_{\max} K_{ads}}\right) \frac{1}{C_e} \tag{6b}$$

where q_e (mg/g) and C_e (mg/g) are the equilibrium adsorption capacity and liquid phase concentration at equilibrium, respectively. $q_{\max}$ (mg/g) is the maximum adsorption capacity when a monolayer is formed on the AN adsorbent, and K_{ads} (L/mg) is the Langmuir adsorption constant. The values of $q_{\max}$ (35.97 mg/g) and K_{ads} (0.01 L/mg) were calculated using a plot of $1/q_e$ vs. $1/C_e$ (Figure 6(a)).

The equilibrium data was well-fitted ($R^2 = 0.9943$) to the Langmuir model. A dimensionless constant called the equilibrium parameter, R_L ($1/(1 + K_{ads} C_0)$), can be used to prove the suitability of AN adsorbent for the removal of MG. The adsorption of any pollutant is regarded favorable if $0 < R_L < 1$, unfavorable if $R_L > 1$, linear if $R_L = 1$, and irreversible if $R_L = 0$. In present the study, the R_L value was found to be 0.49, indicating that AN is a useful material for the adsorption of MG dye.

The Freundlich isotherm assumes that the contaminant is adsorbed on a heterogeneous surface and can be written as shown in Equation (7).

$$q_e = K_F C_e^{1/n} \tag{7}$$

where K_F (L/g) indicates the relative adsorption capacity, and $1/n$ is the heterogeneity factor of adsorption. The equilibrium data fit this model better ($R^2 = 0.99$) than the Langmuir model. This reflects the heterogeneous distribution of active sites and the multilayer coverage of the MG molecules. The constants K_F and $1/n$ were calculated to be 0.87 L/g and 1.74, respectively, which indicates the feasibility of the adsorption of MG by AN. The value of n (the Freundlich exponent) is less than 1 if adsorption is favorable (Hameed *et al.* 2008; Ahmaruzzaman & Gayatri 2010). In the present study, the value of n was 0.58 (Figure 6(b)), which indicates the usefulness of AN for the adsorption of MG.

The Halsey model (Equation (8a)) was used to assess the multilayer adsorption at moderately large distances from the surface. It can be written in a linearized form, as shown in Equation (8b).

$$q_e = \exp\left(\frac{\ln K_H - \ln C_e}{n_H}\right) \tag{8a}$$

$$\ln q_e = \frac{1}{n_H} \ln K_H - \frac{1}{n_H} \ln C_e \tag{8b}$$

where K_H and n_H are Halsey's isotherm constants, which are calculated from the slope and intercept, respectively, of a plot of $\ln C_e$ vs. $\ln q_e$. The values of K_H and n_H were found to be -0.58 and 5.34, respectively, and this model showed the best fit to the adsorption data ($R^2 = 0.99$, Figure 6(c)), confirming the heterogeneous nature of the AN adsorbent.

The physical or chemical nature of MG adsorption onto the surface of AN adsorbent was investigated using the D-R isotherm, as expressed using Equations (9a)–(9c).

$$\ln q_e = \ln q_{DR} - \beta \varepsilon^2 \tag{9a}$$

$$\varepsilon = RT \ln\left[1 + \frac{1}{C_e}\right] \tag{9b}$$

$$E = \frac{1}{\sqrt{-2\beta}} \tag{9c}$$

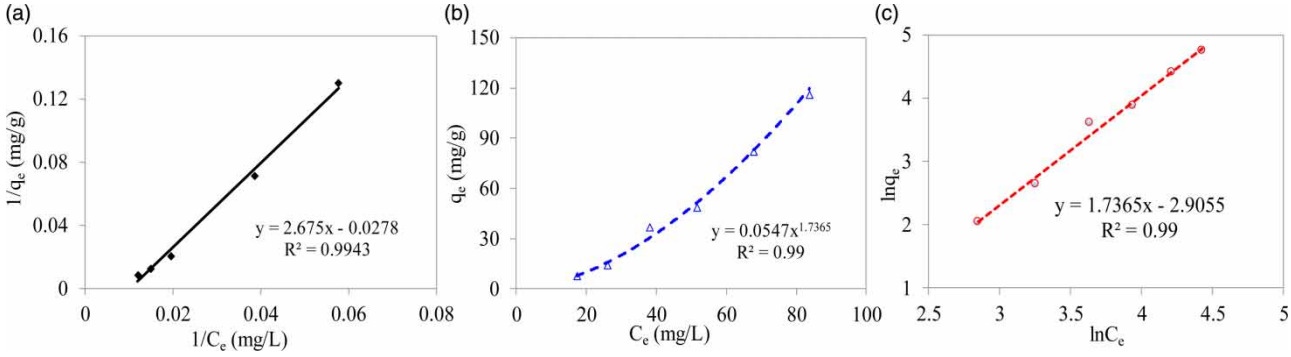

Figure 6 | Langmuir (a), Freundlich (b), and Halsey (c) isotherm plots of the adsorption of MG by AN.

where q_{DR} (mol/g) is the theoretical monolayer sorption capacity, β is the constant of adsorption energy (mol^2/kJ^2), ε is the Polanyi potential, E is the mean free energy of adsorption (kJ/mol), T is the solution temperature (K), and R is the gas constant (8.314 J/mol. K). The values of q_{DR} and β were calculated from the intercept and slope of the plot of lnq_e vs. RT ln$(1 + 1/C_e)$ and were found to be 198.44 mol/g and 0.01 mol^2/kJ, respectively. The R^2 value (0.9611, Figure 7(a)) for the D-R isotherm was lower than that of Langmuir, Freundlich, and Halsey isotherm models. The mean free energy (E) required by one mole of adsorbate to reach the active sites from an infinite distance was calculated to be 6.52 kJ/mol. This indicates physisorption involving Van der Waals forces between the surface of the AN adsorbent and the cationic MG dye molecules, thus supporting the assumption of multilayer adsorption.

The Temkin isotherm model (Equations (10a) and (10b) in linearized form) postulates that (i) the enthalpy of adsorption of all the molecules in the layer decreases linearly rather than logarithmically with coverage (Aharoni & Ungarish 1977), and (ii) the adsorption phenomenon is characterized by the uniform distribution of binding energies at the surface of an adsorbent (Temkin & Pyzhev 1940; Kumar & Gayathri 2009).

$$q_e = \frac{RT}{b_T} \ln (A_T C_e) \tag{10a}$$

$$q_e = B_T \ln A_T + B_T \ln C_e \tag{10b}$$

where A_T (L/g) is the equilibrium binding constant that indicates the maximum bonding energy, and b_T (B_TRT, kJ/mol) is the constant related to the heat of adsorption. The values of A_T and b_T, as calculated from the plot of q_e vs. ln C_e, were found to be 1.3697 L/g and 1.07 kJ/mol, respectively. The Temkin model did not fit the MG adsorption data well, having an R^2 value of 0.9296 (Figure 7(b)). This suggests the nonuniform surface morphology of the AN adsorbent that favors multilayer adsorption.

Pseudo-second-order kinetics

The adsorption of MG by AN was modeled to analyze the rate of MG removal at a concentration of 40 mg/L MG. The pseudo-second-order equation is given in Equation (11).

$$\frac{d_q}{d_t} = k_2 (q_e - q_t)^2 \tag{11}$$

where k_2 (g/mg min) is the rate constant. After the application of boundary limits and integration, the Equation (11) becomes

$$\frac{t}{q_t} = \frac{1}{k_2 q_e^2}. \tag{12}$$

Second-order rate constants were used to calculate the sorption rate using Equation (13).

$$h = k_2 q e^2 \tag{13}$$

A good fit to the experimental data was observed with the pseudo-second-order model ($R^2 = 0.9989$). The calculated adsorption capacity ($q_{e\ cal}$) and k_2 were determined from the slope and intercept of the plot of t/q_t vs. t (Figure 8(a)). The values of k_2 and h were found to be 0.03 g/mg min and 1.56 mg/g min, respectively. However, although the correlation coefficient, R^2, was close to unity, the value of $q_{e\ cal}$ (7.83 mg/g) is not acceptable and demonstrates the relatively

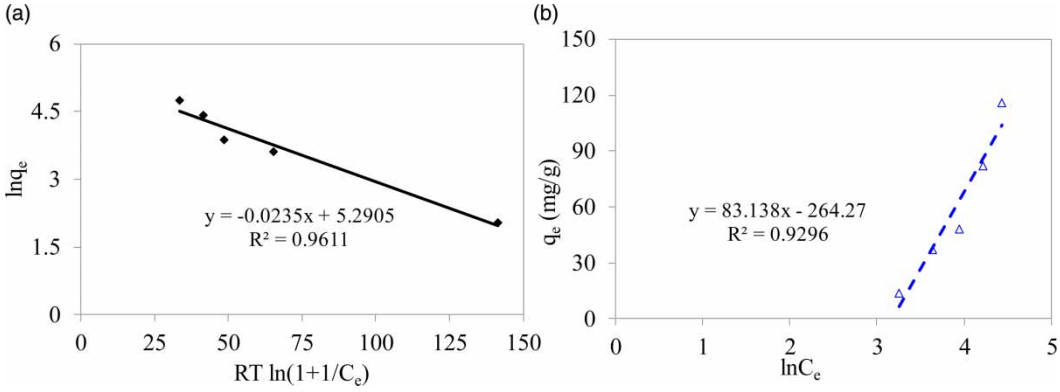

Figure 7 | Dubinin-Radushkevich (a) and Temkin (b) isotherm plots of the adsorption of MG by AN.

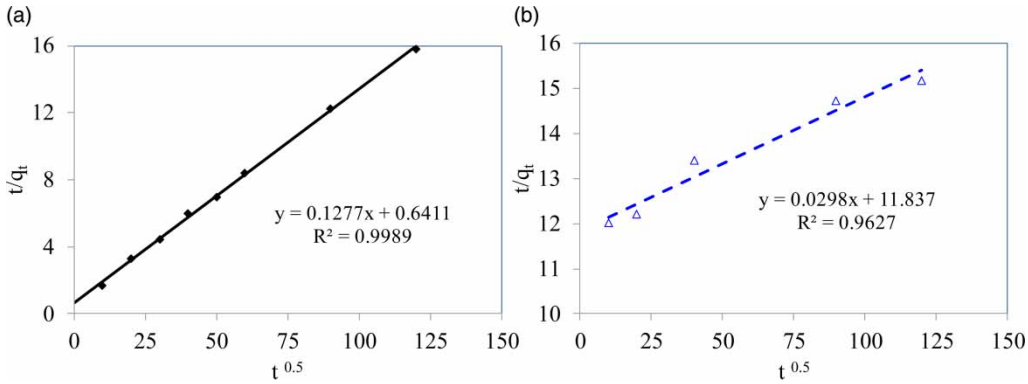

Figure 8 | Pseudo-second order plot (a) and intra-particle diffusion model (b) of the adsorption of MG by AN.

large deviation, almost 50%, from the experimental MG adsorption capacity value (15.18 mg/g). This suggests that chemisorption may not be the only rate limiting step. It also implies that more than one process affects the adsorption of MG onto the surfaces of the AN adsorbent particles.

The intra-particle diffusion model was used to investigate the mechanism and the driving force behind contaminant adsorption. This model can be expressed as Equation (14).

$$q_t = K_{pi}t^{1/2} + C_i \tag{14}$$

where q_t (mg/g) is the adsorption capacity at time t, C_i is the boundary-layer thickness, and K_{pi} (mg/g min$^{0.5}$) is the intra-particle diffusion rate constant. K_{pi} and C_i were calculated from the slope and intercept of the plot of q_t vs. $t^{0.5}$. The value of K_{pi} was determined to be 0.028 mg/g min$^{0.5}$.

According to this model, q_t varies linearly with the square root of time. Although this model showed a poor fit ($R^2 = 0.9627$) to the data compared to the pseudo-second-order model (Figure 8(b)), the larger values of C_i (12.23 mg/g) reflect the contribution of surface diffusion processes in the rate controlling step. Moreover, the intra-particle diffusion model is valid only if q_t vs. $t^{0.5}$ passes through the origin; otherwise, other adsorption mechanisms are involved, alongside the intra-particle diffusion model.

CONCLUSIONS

In this work, the batch adsorption conditions of MG by AN were optimized. An increased removal of MG dye (about 10%) was observed with increasing contact time, from 20 to 240 min, and equilibrium adsorption of MG dye was attained after 40 min. The adsorption of MG was significantly reduced (about 47%) at low pH (4) compared to that at high pH (11). In addition, MG adsorption increased significantly (about 25%) on increasing the speed of agitation from 100 to 220 rpm. Among the other parameters affecting adsorption, a high MG adsorption capacity (about 56%) was observed at a maximum initial MG dye concentration of 200 mg/L compared to that at lower initial MG dye concentration (25 mg/L), indicating the dependency of AN adsorption on the initial adsorbate concentration in the solution. The maximum equilibrium adsorption capacity of AN was 113.26 mg/g at 30 °C. The MG adsorption data indicate multilayer adsorption because the data were fit better by the Freundlich and Halsey models ($R^2 = 0.99$) than by the Langmuir model. Using the D-R model, we confirmed the involvement of physisorption during multilayer adsorption, which was determined from the E value of the D-R model (6.52 kJ/mol). Surface diffusion was found to be a possible mechanism for the adsorption of MG by AN. The MG adsorption reaction was endothermic, based on the enthalpy, and was controlled by the entropy of the system in the T_1 temperature range (30 to 40 °C), while the opposite trend was observed in the T_2 range (40 to 50 °C). Moreover, MG adsorption was found to be nonspontaneous at all temperatures.

ACKNOWLEDGEMENTS

The project was financially supported by King Saud University, Vice Deanship of Research Chairs.

CONFLICT OF INTEREST

Authors declare no conflict of interest.

REFERENCES

Aharoni, C. & Ungarish, M. 1977 Kinetics of activated chemisorption. Part 2.–Theoretical models. *Journal of the Chemical Society, Faraday Transactions 1: Physical Chemistry in Condensed Phases* **73** (0), 456–464.

Ahmaruzzaman, M. & Gayatri, S. L. 2010 Activated tea waste as a potential low-cost adsorbent for the removal of p-Nitrophenol from wastewater. *Journal of Chemical & Engineering Data* **55** (11), 4614–4623.

Akar, E., Altinişik, A. & Seki, Y. 2013 Using of activated carbon produced from spent tea leaves for the removal of malachite green from aqueous solution. *Ecological Engineering* **52**, 19–27.

Amin, M., Alazba, A. & Shafiq, M. 2015 Adsorptive removal of reactive black 5 from wastewater using bentonite clay: isotherms, kinetics and thermodynamics. *Sustainability* **7** (11), 15302–15318.

Amin, M. T., Alazba, A. A. & Shafiq, M. 2016 Adsorption of copper (Cu^{2+}) from aqueous solution using date palm trunk fibre: isotherms and kinetics. *Desalination and Water Treatment* **57** (47), 22454–22466.

Azbar, N., Yonar, T. & Kestioglu, K. 2004 Comparison of various advanced oxidation processes and chemical treatment methods for COD and color removal from a polyester and acetate fiber dyeing effluent. *Chemosphere* **55** (1), 35–43.

Baek, M.-H., Ijagbemi, C. O., O, S.-J. & Kim, D.-S. 2010 Removal of Malachite Green from aqueous solution using degreased coffee bean. *Journal of Hazardous Materials* **176** (1–3), 820–828.

Culp, S. J., Blankenship, L. R., Kusewitt, D. F., Doerge, D. R., Mulligan, L. T. & Beland, F. A. 1999 Toxicity and metabolism of malachite green and leucomalachite green during short-term feeding to Fischer 344 rats and b6c3f1 mice. *Chemico-Biological Interactions* **122** (3), 153–170.

Dubinin, M. M. & Radushkevich, L. V. 1947 Equation of the characteristic curve of activated charcoal. *Proceedings of the Academy of Sciences of the USSR, Physical Chemistry Section* **55**, 331–333.

Fil, B. A., Yilmaz, M. T., Bayar, S. & Elkoca, M. T. 2014 Investigation of adsorption of the dyestuff astrazon red violet 3rn (basic violet 16) on montmorillonite clay. *Brazilian Journal of Chemical Engineering* **31** (1), 171–182.

Freundlich, H. M. F. 1906 Over the adsorption in solution. *Journal of Physical Chemistry* **57**, 385–471.

Gao, B.-Y., Yue, Q.-Y., Wang, Y. & Zhou, W.-Z. 2007 Color removal from dye-containing wastewater by magnesium chloride. *Journal of Environmental Management* **82** (2), 167–172.

Ghoreishi, S. M. & Haghighi, R. 2003 Chemical catalytic reaction and biological oxidation for treatment of non-biodegradable textile effluent. *Chemical Engineering Journal* **95** (1–3), 163–169.

Guo, Y., Yang, S., Fu, W., Qi, J., Li, R., Wang, Z. & Xu, H. 2003 Adsorption of malachite green on micro- and mesoporous rice husk-based active carbon. *Dyes and Pigments* **56** (3), 219–229.

Gupta, V. K., Mittal, A., Krishnan, L. & Gajbe, V. 2004 Adsorption kinetics and column operations for the removal and recovery of malachite green from wastewater using bottom ash. *Separation and Purification Technology* **40** (1), 87–96.

Halsey, G. 1948 Physical adsorption on non-uniform surfaces. *The Journal of Chemical Physics* **16** (10), 931–937.

Hameed, B. H. & El-Khaiary, M. I. 2008 Malachite green adsorption by rattan sawdust: isotherm, kinetic and mechanism modeling. *Journal of Hazardous Materials* **159** (2–3), 574–579.

Hameed, B. H., Chin, L. H. & Rengaraj, S. 2008 Adsorption of 4-chlorophenol onto activated carbon prepared from rattan sawdust. *Desalination* **225** (1–3), 185–198.

Inbaraj, B. S. & Sulochana, N. 2002 Basic dye adsorption on a low cost carbonaceous sorbent-kinetic and equilibrium studies. *Indian Journal of Chemical Technology* **9**, 201–208.

Jain, M., Mudhoo, A. & Garg, V. K. 2011 Swiss blue dye sequestration by adsorption using *Acacia nilotica* sawdust. *International Journal of Environmental Technology and Management* **14** (1–4), 220–237.

Janoš, P., Buchtová, H. & Rýznarová, M. 2003 Sorption of dyes from aqueous solutions onto fly ash. *Water Research* **37** (20), 4938–4944.

Kant, R. 2012 Adsorption of dye eosin from an aqueous solution on two different samples of activated carbon by static batch method. *Journal of Water Resource and Protection* **04** (02), 93–98.

Kapdan, I. K., Kargia, F., McMullan, G. & Marchant, R. 2000 Effect of environmental conditions on biological decolorization of textile dyestuff by C. versicolor. *Enzyme and Microbial Technology* **26** (5–6), 381–387.

Kattri, S. & Singh, M. 1999 Adsorption of basic dyes from aqueous solution by natural adsorbent. *Indian Journal of Chemical Technology* **6**, 112–116.

Khattri, S. D. & Singh, M. K. 2000 Colour removal from synthetic dye wastewater using a bioadsorbent. *Water, Air, and Soil Pollution* **120** (3–4), 283–294.

Kumar, P. S. & Gayathri, R. 2009 Adsorption of Pb2+ ions from aqueous solutions onto bael tree leaf powder: isotherms, kinetics and thermodynamics study. *J. Eng. Sci. Technol* **4** (4), 381–399.

Kumar, K. V., Sivanesan, S. & Ramamurthi, V. 2005 Adsorption of malachite green onto Pithophora sp., a fresh water algae: equilibrium and kinetic modelling. *Process Biochemistry* **40** (8), 2865–2872.

Langmuir, I. 1918 The adsorption of gases on plane surfaces of glass, mica and platinum. *Journal of the American Chemical Society* **40** (9), 1361–1403.

Lu, K., Zhang, X.-L., Zhao, Y.-L. & Wu, Z.-L. 2010 Removal of color from textile dyeing wastewater by foam separation. *Journal of Hazardous Materials* **182** (1–3), 928–932.

Pan, X. & Zhang, D. 2009 Removal of malachite green from water by Firmiana simplex wood fiber. *Electronic Journal of Biotechnology* **12** (4), 1–10.

Rajeshwarisivaraj, & Subburam, V. 2002 Activated parthenium carbon as an adsorbent for the removal of dyes and heavy metal ions from aqueous solution. *Bioresource Technology* **85** (2), 205–206.

Riera-Torres, M., Gutiérrez-Bouzán, C. & Crespi, M. 2010 Combination of coagulation–flocculation and nanofiltration techniques for dye removal and water reuse in textile effluents. *Desalination* **252** (1–3), 53–59.

Shakoor, S. & Nasar, A. 2016 Removal of methylene blue dye from artificially contaminated water using citrus limetta peel waste as a very low cost adsorbent. *Journal of the Taiwan Institute of Chemical Engineers* **66**, 154–163.

Shanmugaprakash, M., Sivakumar, V., Manimaran, M. & Aravind, J. 2014 Batch and dynamics modeling of the biosorption of Cr (VI) from aqueous solutions by solid biomass waste from the biodiesel production. *Environmental Progress & Sustainable Energy* **33** (2), 342–352.

Srivastava, S., Sinha, R. & Roy, D. 2004 Toxicological effects of malachite green. *Aquatic Toxicology* **66** (3), 319–329.

Sugumar, W. & Gopalan, R. 2000 Removal of dyestuffs from aqueous solutions using maize cob. *Asian Journal of Chemistry* **12** (3), 668–674.

Temkin, M. & Pyzhev, V. 1940 Kinetics of the synthesis of ammonia on promoted iron catalysts. *Catalysts Acta Physiochim USSR* **12**, 217–222.

Wei, J., Gao, B., Yue, Q. & Wang, Y. 2009 Effect of dosing method on color removal performance and flocculation dynamics of polyferric-organic polymer dual-coagulant in synthetic dyeing solution. *Chemical Engineering Journal* **151** (1–3), 176–182.

Wu, Y., Fan, Y., Zhang, M., Ming, Z., Yang, S., Arkin, A. & Fang, P. 2016 Functionalized agricultural biomass as a low-cost adsorbent: utilization of rice straw incorporated with amine groups for the adsorption of Cr(VI) and Ni(II) from single and binary systems. *Biochemical Engineering Journal* **105** (Part A), 27–35.

Yang, X. & Al-Duri, B. 2005 Kinetic modeling of liquid-phase adsorption of reactive dyes on activated carbon. *Journal of Colloid and Interface Science* **287** (1), 25–34.

Yetilmezsoy, K. & Sakar, S. 2008 Improvement of COD and color removal from UASB treated poultry manure wastewater using Fenton's oxidation. *Journal of Hazardous Materials* **151** (2–3), 547–558.

Yonar, M. E. & Yonar, S. M. 2010 Changes in selected immunological parameters and antioxidant status of rainbow trout exposed to malachite green (Oncorhynchus mykiss, Walbaum, 1792). *Pesticide Biochemistry and Physiology* **97** (1), 19–23.

Zhang, J., Li, Y., Zhang, C. & Jing, Y. 2008 Adsorption of malachite green from aqueous solution onto carbon prepared from Arundo donax root. *Journal of Hazardous Materials* **150** (3), 774–782.

First received 13 October 2016; accepted in revised form 5 June 2017. Available online 20 June 2017